1

Influence of process parameters including the confining magnetic field of a plasma beam source on the deposition of N-doped hydrogenated carbon films

K. Petrikowski[1], M. Fenker[1*] and H.Kaßner[1]

[1]fem Forschungsinstitut, Katharinenstraße 13-17, 73525 Schwäbisch Gmünd

(Received: 24. Oct. 2023, Accepted: 14. Nov. 2023, Published online: 15. Nov. 2023)

Electrically conductive nitrogen-doped hydrogenated carbon films (a-C:H:N) were deposited using a nitrogen-acetylene gas mixture by plasma-assisted chemical vapor deposition (PACVD). A capacitively coupled plasma beam source was used for the depositions. The plasma is excited by a radio-frequency (RF) discharge and confined by Helmholtz magnetic coils, resulting in an increase in plasma density. The ion energy, as well as the deposition rate, can be controlled by the choice of the size of the coupling electrode, i.e. the ratio of cathode-to-anode area, the electric current at the Helmholtz magnet coils, the total gas pressure and the RF power. The interdependence of these process parameters on the ion energy and the deposition rate has been studied in detail in this work. Hardness and electrical resistivity were measured on the deposited a-C:H:N films.

© G-Labs 2023

(DOI: 10.31281/jtsp.v4i1.29)

*fenker@fem-online.de

I. Introduction

Fuel cells are a promising and environmentally friendly technology for the conversion of chemical energy into electrical energy that has received immense attention in recent years as an alternative to conventional fossil energy sources. The advantage of fuel cells compared to other renewable energy sources such as solar or wind energy is the continuous production of electrical energy regardless of weather conditions. However, the electrical efficiency of a polymer electrolyte fuel cell (PEMFC) is only about 40-60% [1], [2]. Efforts are being made to increase the efficiency, performance and service life of fuel cells (FCs). One component of PEM fuel cells which has to be improved is the bipolar plate (BP). In the last years, graphite/polymer compound BPs have been replaced by metallic BPs. With metallic BPs, the weight of the FC stack can be lower and the size can be smaller. BPs made of stainless steel are especially interesting, due to the formability, abundance and low costs [3]. However, this metal needs to be coated with highly conductive and corrosion resistant materials, since in the harsh environment of a fuel cell the stainless steel passivates and thus the contact resistance increases. In addition, the passive film can dissolve and reform when the ambient conditions change, resulting in the release of metal ions and impurities. These species can poison the solid polymer electrolyte as well as the catalyst layer, resulting in inferior fuel cell performance.

For this purpose, nitrogen-doped hydrogenated carbon films (a-C:H:N, abbreviation according to [4]) are of particular interest as they exhibit high electrical conductivity due to the presence of nitrogen atoms and are also chemically inert and therefore corrosion resistant. To increase the deposition rate of a-C:H:N films by optimizing PACVD process parameters and keep – or even improve – the high electrical conductivity of the

films is the goal of this study. To obtain electrically conductive carbon coatings by the PACVD method 3 different process routes alone and in combination have been followed [5]:

1. Varying the kinetic energy of the impinging species by changing the total pressure,
2. Increasing the substrate temperature,
3. Adding N_2 to the C_2H_2 precursor gas.

The first two routes can lead to a graphitization of the carbon films, i.e. by increasing the sp^2 phase and decreasing the sp^3 phase of the carbon bonding in the carbon matrix [6], [7]. The kinetic energy of the ionic species arriving at the growing film surface will strongly depend on the total pressure in the vacuum chamber. The number of collisions (ion-neutral species collision), the ionic species will face during travelling between PBS and substrate surface, can be estimated from the mean free path length, λ [5]. For example, λ will assumes values of about 20 cm at 0.04 Pa (4×10^{-4} mbar) and 0.9 cm at 0.09 Pa (9×10^{-4} mbar) for the lowest and the highest total pressure applied in this study. The third route is reported to dope the a-C:H matrix by nitrogen, but also increases the amount of sp^2 phase [8]. Silva et al. reported that the addition of N can increase the electrical conductivity of a-C:H films by a) doping the a-C:H film by raising the Fermi level towards the conduction band, or by b) graphitization of the bonding and therefore narrowing the band gap [8]. Furthermore, they showed that there are nine possible binding modes of nitrogen in an a-C:H:N film, but only three of them contribute to the electrical conductivity. Doping of a-C:H only takes place, when there still exists an unpaired electron in the nitrogen atom after incorporation into the a-C:H matrix. This is the reason why nitrogen is a weak dopant for a-C:H films.

II. Experimental Setup

The depositions have been conducted in a vacuum system, called Cobra Cube CC11 (CCR GmbH, Fig. 1). The system, designed for PACVD (plasma-enhanced chemical vapor deposition) processes, was used to deposit the a-C:H:N films. For this purpose, an N_2/C_2H_2 gas mixture was activated in the plasma of a capacitively coupled plasma beam source PBS 200 (HS-Group GmbH) (Fig. 2).

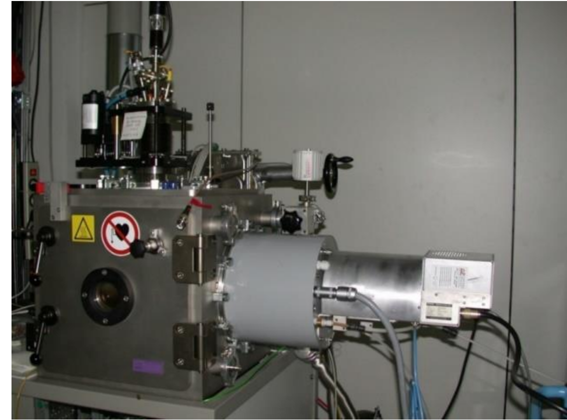

Figure 1: Vacuum system of the type Cobra Cube CC11 (CCR GmbH) with a capacitively coupled plasma beam source PBS 200 (HS-Group GmbH).

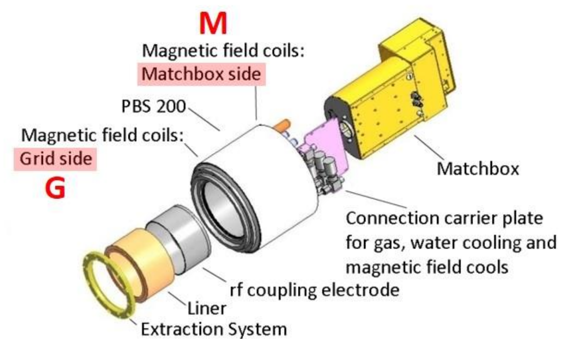

Figure 2: Exploded view of the capacitively coupled plasma beam source PBS 200 (HS-Group GmbH, adapted from [9])

The plasma beam source provides an electrically neutral plasma which is excited by a radio frequency (f = 27.12 MHz) and confined by a pair of Helmholtz magnetic coils to achieve a high plasma density. One coil is aligned to the grid and one to the side of the matchbox, abbreviated by G and M, respectively. By choosing the size i.e. the area of the coupling electrode (cathode-to-anode area ratio, A_C/A_A), the extraction energy of the ions, i.e., the ion energy, can be changed [10], [11]. According to equation (1) the change of the cathode-to-anode area ratio A_C/A_A has a direct influence on the voltage drop at the anode, U_A. This voltage drop U_A is equal to the potential difference between the plasma and the extraction grid and is responsible for the acceleration of the ions.

$$\frac{U_A}{U_C} = \left(\frac{A_C}{A_A}\right)^n \quad (1)$$

U_C is the voltage drop at the cathode and n is the pressure dependent exponent, which can assume

values of 1 … 4 (1: high pressures, 4: low pressures) [12].

Two different coupling electrodes, i.e. A_C/A_A ratios, have been deployed. According to equation (1) the energy of the extracted ions is higher for a larger cathode A_C. The areas and area ratio of small and large coupling electrode are listed in table 1. Obviously, the A_C/A_A ratio of the large coupling electrode is about a factor of 5 higher compared to the small coupling electrode.

Electrode	small coupling electrode	large coupling electrode
A_C (cm^2)	680	919
A_A (cm^2)	318	78
A_C/A_A	2.1	11.8

Table 1: Areas and area ratio of small and large coupling electrode.

Figs. 3a and 3b show the small coupling electrode and the large coupling electrode. By appropriate selection of the coupling electrode, the currents of the G and M magnetic coils, the substrate temperature, the total pressure, and the N_2 gas flow, conductive carbon films can be deposited. At the lowest adjustable total pressure of $2x10^{-4}$ mbar, almost no collisions of the ions with the residual gas on the way to the substrate (distance 8 cm) can be expected. At an average total pressure ($1x10^{-3}$ mbar), the ions are already significantly slowed down, and at a high total pressure ($1x10^{-2}$ mbar), the ions are almost thermalized. Therefore, the ion energy of the particles at the substrate location can be significantly affected by a change in total pressure. The stationary substrate holder, made specifically for these coatings, is heated by a BORALECTRIC® heater. This heater consists of a combination of pyrolytic boron nitride and a dielectric ceramic with pyrolytic graphite. Temperatures of over 1000°C can be achieved with this resistive heater.

Figure 3a: Photo of liner and in the background the small coupling electrode with disassembled gas deflection plate connected to the plasma beam source.

Figure 3b: Photo of large coupling electrode of the plasma beam source

In addition, by regulating the current of the G and M magnetic coils of the plasma beam source, the plasma can be "shaped" and thus the properties of the plasma can also be changed. In Fig. 4a and Fig. 4b, the influence of the magnetic coils setting can be easily observed by looking at the shape of the plasma. In Fig. 4a, a current of 0 A was applied to the magnetic coil on the G side and a current of 10 A (G0M10) on the M side. This gives a very wide plasma beam. In Fig. 4b, a current of 0 A was applied to the magnetic coil on the G side and a current of 0.7 A (G0M0.7) on the M side. The plasma beam with a diameter of 16 cm at the beam exit is extremely focused and hits the substrate at a distance of 28 cm away with a beam diameter of about 2 cm.

Figure 4a: Non-focused plasma beam of the plasma beam source (right: plasma beam source; left: substrate) with the large coupling electrode, a power of 400 W, a pressure of $2x10^{-4}$ mbar and a magnetic coil setting of G0M10.

Figure 4b: Focused plasma beam of the plasma beam source (right: plasma beam source; left: substrate) with the large coupling electrode, a power of 400 W, a pressure of $2x10^{-4}$ mbar and a magnetic coil setting of G0M0.7.

The deposition rate was determined with an STM-2 USB thin film rate/thickness monitor from INFICON. The deposition rate is measured during the coating process. For this purpose, an oscillating quartz crystal monitor (QCM) is brought into resonance and exposed to the coating material. The change in coating mass (Δm) can be determined by the frequency shift in the resonance frequency of the QCM. The change in resonance frequency with respect to the frequency itself is small. To reduce the temperature effect, the sensor is water-cooled. The change in resonance frequency can be calculated by Sauerbrey's equation [13]:

$$\Delta f = \frac{\Delta m \times F^2}{N \times S \times r} \qquad (2)$$

where Δf is the change in frequency, F is the fundamental frequency of the QCM, N is a frequency constant, S is the surface area and r is the density of the crystal.

In addition to the nitrogen doping and deposition at elevated temperature, a high ion energy is crucial for the deposition of electrically conductive carbon films. The ion energy was measured with a Faraday cup. The Faraday cup consists of a metal pot with a deep hole. The electrical charge introduced by the ions impinging on the bottom of the cup is collected by an electrometer. To measure the ion energy, an opposing electric field (up to +1100 V) is applied, thus decelerating the ions. By means of the derivative of the recorded current-voltage curve, the maximum of the ion energy can be determined. As the ions strike the metal ground, electrons are also knocked out of the metal. To prevent these electrons from contributing to the charge, a reverse voltage of -150 V is applied to a suppressor electrode. In addition to recording the ion energy, the current density can also be acquired. The current density can be calculated from the initial current of the ion energy measurement and the orifice area of the Faraday cup.

The Vickers hardness was determined by means of an instrumented indentation test according to DIN EN ISO 14577-1 using a test apparatus from Helmut Fischer GmbH of the type FISCHERSCOPE H100. A Vickers indenter at a maximum test load of 2 mN was indented with a loading, holding and unloading time of 10 s each. The Vickers hardness was reported as the average of 10 - 20 individual measurements. For the measurement of the hardness, the layer thickness of the a-C:H:N layers deposited on silicon wafers should be approx. 1 µm in order not to violate the Bückle rule, which states that the penetration depth h_{max} in the hardness measurement must not be greater than 10 % of the layer thickness. The Bückle rule could not always be followed, since thinner layers (< 1 µm) had to be deposited in some cases due to adhesion problems. Electrical resistance of the films was measured using the 4-point method with a Keithley model 2000 digital multimeter.

III. Results

III.a) Deposition rate as a function of the magnetic field coil settings

The QCM was used to measure the deposition rates for the small and large coupling electrode at

 © G-Labs 2023

different magnetic coil settings at the G-side and M-side of the plasma beam source. A deposition pressure of $4x10^{-4}$, $7x10^{-4}$ and $9x10^{-4}$ mbar was selected for the a-C:H:N depositions with an N_2/C_2H_2 ratio of 0.78. A power of 300 W was applied to the plasma beam source and the current at the magnetic coils was varied from 0 A to 12 A. Due to strong focusing of the plasma beam at certain magnetic coil settings, a very small distance of 4 cm between the QCM and the grid G (tungsten grid = extraction grid) of the plasma beam source was chosen to minimize the influence of the focusing on the measurement of the deposition rate. Figs. 5a and 5b show the deposition rates as a function of the magnetic coil settings on the G and M sides of the plasma beam source for the small and large coupling electrode at different pressures. From the graphs, it can be recognized that the deposition rates strongly depend on the magnetic coil settings and increase with increasing pressure. For the small coupling electrode, the deposition rate is about twice as high as for the large coupling electrode. The reddish-brown areas relate to magnetic coil settings where the plasma beam source did not run stable and failed more often. Deposition rates in the range 1.3 µm/h (G4M7) to 2.4 µm/h (G12M0) were determined for the small coupling electrode. In comparison, lower deposition rates in the range 0.5 µm/h (G4M7) to 1.2 µm/h (G11M5) were measured with the large coupling electrode. In a previous paper by our group [5], the highest deposition rates measured at an N_2/C_2H_2 ratio of 0.78, with the small coupling electrode, a magnetic coil setting of G4M7 and a power of 300 W was 0.8 µm/h but at a total pressure of $1x10^{-2}$ mbar (1 Pa).

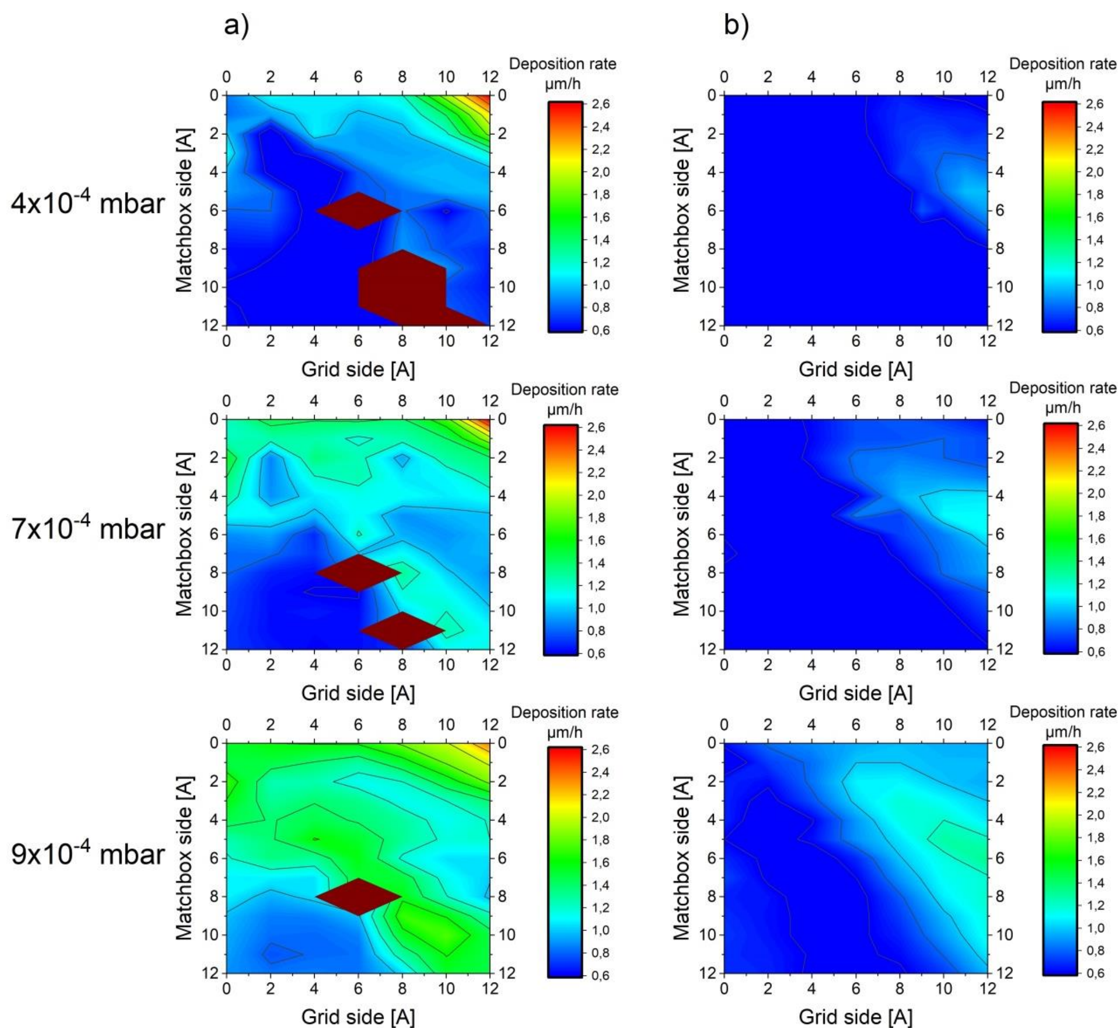

Figure 5: Deposition rate at 300 W as a function of pressure and magnetic coil settings on the G and M sides for a) the small coupling electrode and b) the large coupling electrode.

 © G-Labs 2023

III.b) Deposition rate as a function of RF power

Fig. 6 shows the dependence of the deposition rate measured with the QCM on the RF power of the plasma beam source. The deposition rate was determined at a deposition pressure of $4x10^{-4}$ mbar and an N_2/C_2H_2 ratio of 0.78. The power at the plasma beam source was gradually ramped up from 150 to 1000 W. The magnetic coil settings with in each case highest deposition rate were selected for the two coupling electrodes. However, due to a significant heat generation at the magnetic coils, the current for the small coupling electrode at the G-side was reduced from 12 A to 10 A and therefore a magnetic coil setting of G10M0 was used. As a result, the deposition rate is approx. 0.7 µm/h lower than with the magnetic coil setting for the highest deposition rate with G12M0. For the large coupling electrode, the magnetic coil setting G11M5 was chosen. From the image it can be seen on the one hand that with the small coupling electrode the deposition rate is twice as high as with the large coupling electrode and on the other hand that an increase in power does not result in an increase in deposition rate. It must be taken into account that both neutral and ionized species are measured with the QCM. Therefore, the deposition rate depends mainly on the precursor flow (acetylene) i.e. the resulting pressure. As reported below in section III d (Fig. 8), the applied RF power leads to an increase of the measured current density, i.e., the ionization of the gas species. Furthermore, the ion energy increases steeply with the RF power. This increase is significantly steeper for the large coupling electrode than for the small one. The steep increase in ion energy with increasing power has implications for the deposition rate of the a-C:H:N films. According to Y. Yamamura et al. [14], the sputtering rate increases with increasing ion energy. The sputtering yield for C^+ in C (graphite) doubles from 0.2 to about 0.4 when the ion energy is increased from 500 eV to 2000 eV. Even if an increased flux of layer-forming species were to be produced with RF power, the increased ion energy or sputtering yield may negate the deposition rate benefit. The resulting film growth is the balance of instantaneous film growth and resputtering. Furthermore, with ionized nitrogen (N^{2+}, N^+) the problem of chemical sputtering occurs [5], [15], [16]. This also leads to an increased resputtering rate. These two effects probably contribute to the fact that the deposition rate, as shown in Fig. 6, does not increase with an increase in RF power, but remains approximately constant (small coupling electrode) or even decreases (large coupling electrode).

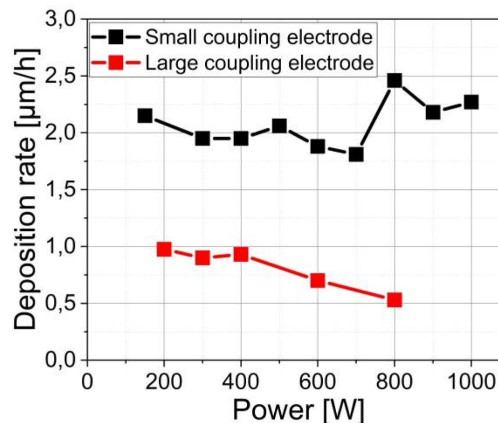

Figure 6: Dependence of deposition rate on the power of the plasma beam source at a coating pressure of $4x10^{-4}$ mbar with a magnetic coil settings for the small coupling electrode with G10M0 and for the large coupling electrode with G11M5.

III.c) Ion energy as a function of the magnetic coil settings

The Faraday Cup was used to determine the ion energy (in eV) of the ionized film-forming species as a function of the magnetic coil settings on the G and M sides of the plasma beam source for the small and large coupling electrode at a coating pressure of $4x10^{-4}$, $7x10^{-4}$ and $9x10^{-4}$ mbar and an N_2/C_2H_2 ratio of 0.78. A power of 150 W was chosen for the plasma beam source since high ion energies were expected for the large coupling electrode and the measurement range is limited by the instrument to a decelerating voltage of +1100 V. In addition, magnetic coil settings were used which are in the range of the highest deposition rate. In Fig. 7, the ion energies for the small and large coupling electrode are shown as a function of the magnetic coil settings and the deposition pressure. From the graphs in Fig. 7a it can be observed that for the small coupling electrode the ion energy decreases with increasing pressure. A maximum ion energy of 555 eV could be achieved with a magnetic coil setting of G10M3 at a pressure of $4x10^{-4}$ mbar. In Fig. 7b the influence of the coating pressure on the ion energy is not clearly visible for the large coupling electrode. A maximum ion energy of 900 eV could be achieved at a magnetic coil setting of G9M7. Anyway, the influence of the magnetic field on the ion energies contributes to only about 10%. Comparing the ion energies in Figs.

 © G-Labs 2023

7a and 7b with the determined deposition rates in Figs. 5a and 5b, it can be concluded that low deposition rates were achieved with high ion energies. This effect was explained in the previous section III b. and is related to the increased resputtering of the growing film at higher ion energies and the chemical sputtering by nitrogen species. It was also found that almost twice as high ion energies were achieved with the large coupling electrode than with the small coupling electrode. This fact can be understood from equation (1). The accelerating voltage, U_A, is increasing with increasing A_C/A_A ratio.

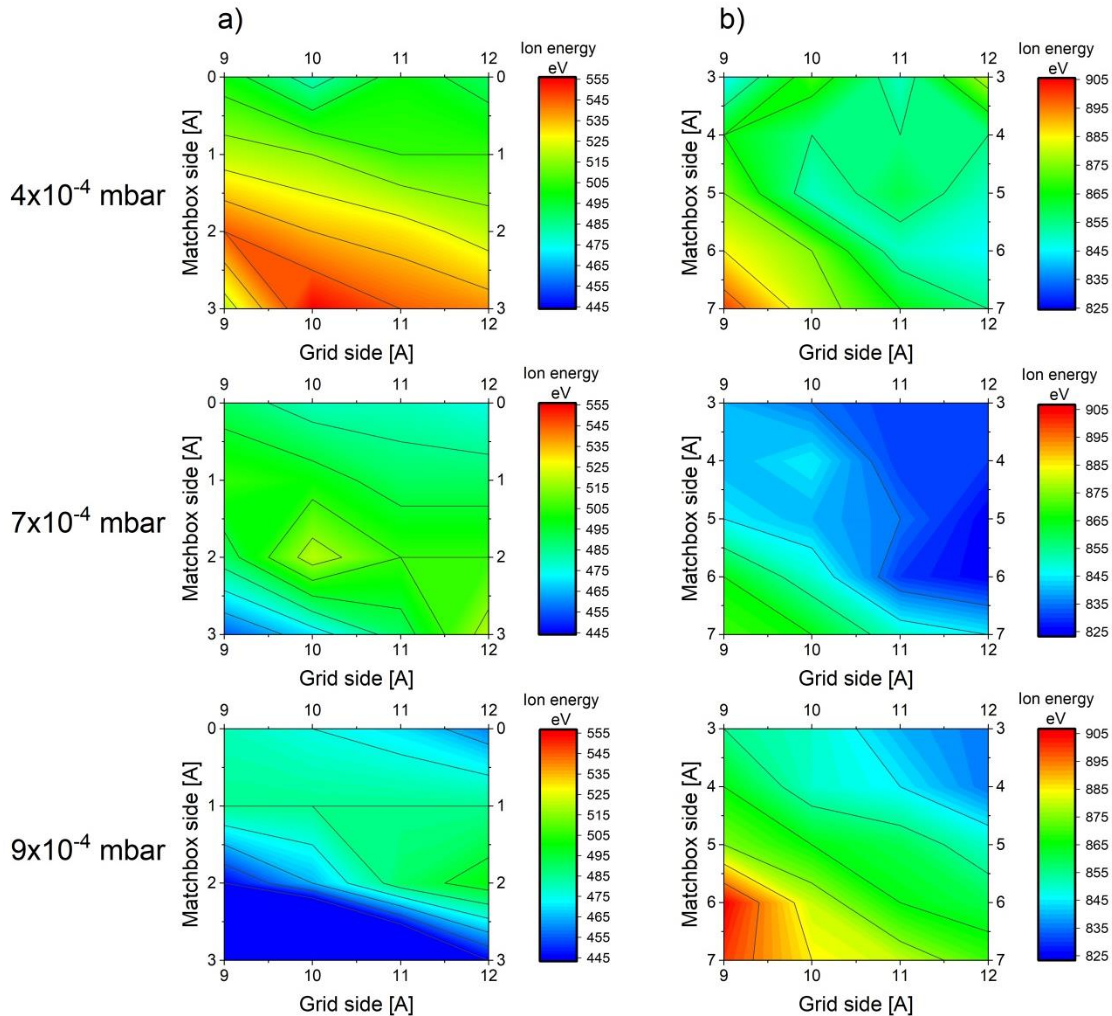

Figure 7: Ion energy at 150 W as a function of pressure and magnetic coil settings at the G and M sides for a) the small coupling electrode and b) the large coupling electrode.

III.d) Ion energy and current as a function of RF power

Figs. 8a and 8b show the dependence of ion energy and current density on RF power for the small coupling electrode with magnetic coil setting G10M0 and for the large coupling electrode with magnetic coil setting G11M5 at a pressure of $4x10^{-4}$ mbar. The settings of the magnetic coils were chosen for a high deposition rate. The power was gradually ramped up from 150 W. For the large coupling electrode, the power increase had to be stooped at 300 W, due to the limitation of the range of the measurement instrument at +1100 V. With increasing power, the ion energy increases, whereby higher ion energies can be achieved with the large coupling electrode. For the small coupling electrode, an ion energy >1100 eV was achieved only at a power of >700 W, while for the large coupling electrode >1100 eV were already achieved at a power of 300 W. At a power of e.g. 300 W, the current density for the small coupling electrode is 0.55 mA/cm² and for the large coupling electrode 0.2 mA/cm². This shows that with the small coupling electrode lower ion energies but higher current densities can be achieved, while the large coupling electrode delivers higher ion energies but lower current densities.

 © G-Labs 2023

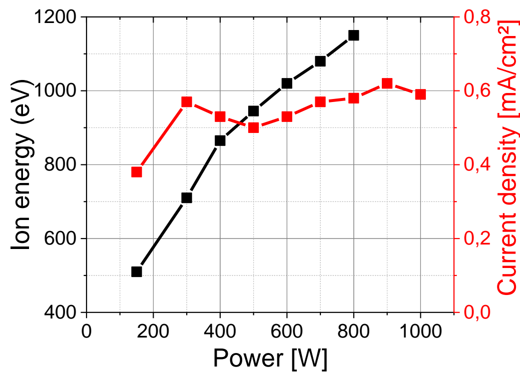

Figure 8a: Ion energy and current density for the small coupling electrode as a function of power at a magnetic coil setting of G10M0 and a pressure of $4x10^{-4}$ mbar.

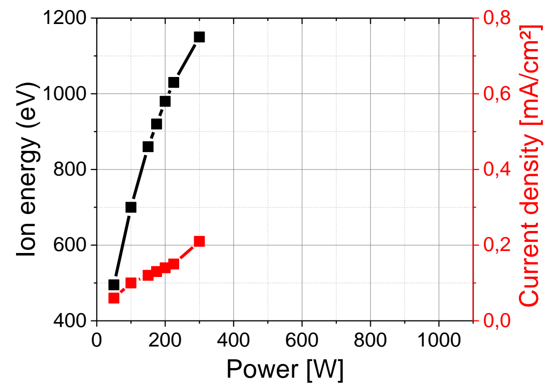

Figure 8b: Ion energy and current density for the large coupling electrode as a function of power at a magnetic coil setting of G11M5 and a pressure of $4x10^{-4}$ mbar.

III.e) Hardness as a function of pressure

Fig. 9 shows the hardness of the a-C:H:N films deposited on silicon wafers as a function of pressure for the small and large coupling electrode with magnetic coil settings for a low and a high deposition rate. The power and deposition time were adjusted in each case to achieve an ion energy >1000 eV and a film thickness of ~1µm. The distance from the substrate holder to the extraction grid of the plasma beam source was 8 cm. The film hardness was in the range of 700 to 1600 HV. The hardness of the a-C:H:N films deposited with the small coupling electrode is lower compared to the large coupling electrode regardless of the coil settings. In addition, the hardness with magnetic coil setting for a high deposition rate (G10M0 and G11M5) is about 200 HV lower for the small coupling electrode and about 200-300 HV higher for the large coupling electrode than with the magnetic coil setting with a low deposition rate (G4M7). In all measurement curves, an increase in hardness with pressure can be observed. This observation is due to the high ion energy of the species. As described in the introduction, the mean free path length, λ, assumes values between 0.9 and 20 cm for a total pressure in the range of $9x10^{-4}$ mbar and $4x10^{-4}$ mbar. Therefore, an increase in pressure in this pressure range slows down the species considerably. According to J. Robertson [17], at ion energies > 100 eV/C atom, the sp^3 structure is already in the relaxation region due to thermally activated diffusion. However, an increased pressure slows down the film-forming species on their way to the substrate by collisions. Thus, the ion energy per C atom decreases and approaches somewhat the hardness maximum at about 100 eV/C atom.

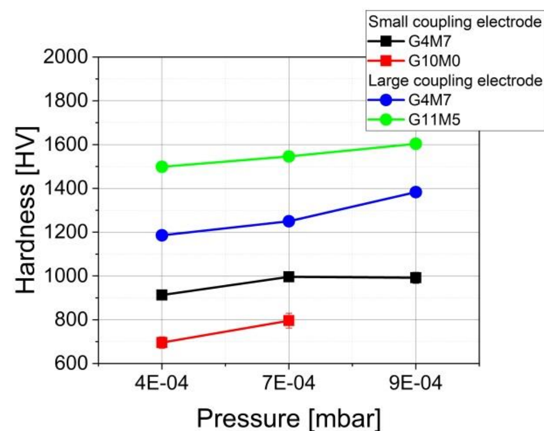

Figure 9: Hardness as a function of pressure for the small and large coupling electrode for magnetic coil settings with a high deposition rate (G10M0 and G11M5) compared to a coil setting with a low deposition rate (G4M7).

III.f) Electrical resistance as a function of substrate temperature for the small coupling electrode

Fig. 10 shows the electrical resistance of the a-C:H:N films deposited on Kapton foil as a function of substrate temperature at a pressure of $4x10^{-4}$ mbar, a power of 300 W

and with the magnetic coil setting G4M7. As can be seen from the graph, there is a jump in electrical resistance above 215 °C. From here on, the a-C:H:N layer becomes an order of magnitude more conductive. This corresponds to the transition temperature T1 (160-330°C) as reported by S. Sattel et al. [6], [7] and results from the thermally induced graphitization of the layers.

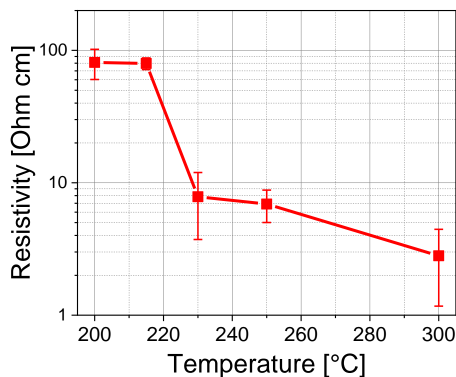

Figure 10: Electrical resistance of a-C:H:N film deposited on Kapton tape as a function of substrate temperature at a pressure of $4x10^{-4}$ mbar, a power of 300 W and a magnetic coil setting of G4M7 with the small coupling electrode.

III.g) Electrical resistance as a function of pressure

Fig. 11 shows the electrical resistivity of the a-C:H:N films deposited on Kapton tape at a substrate temperature of ~270°C as a function of pressure for the small and large coupling electrode for magnetic coil settings for a high (G10M1, G11M5) as well as for a low (G4M7) deposition rate. In each case, the power was adjusted to achieve an ion energy >1000 eV. The distance from the substrate holder to the extraction grid of the plasma beam source was 8 cm. With increasing pressure, the electrical resistivity decreases and is a factor of 2-5 lower for the magnetic coil setting with a high deposition rate for the small coupling electrode than for the large coupling electrode. The electrical resistivity of the a-C:H:N films deposited with magnetic coil settings for low deposition rates is higher than for the magnetic coil settings for high deposition rates. This is an important result as low electrical resistance and high deposition rates are required to transfer this coating technology to industry.

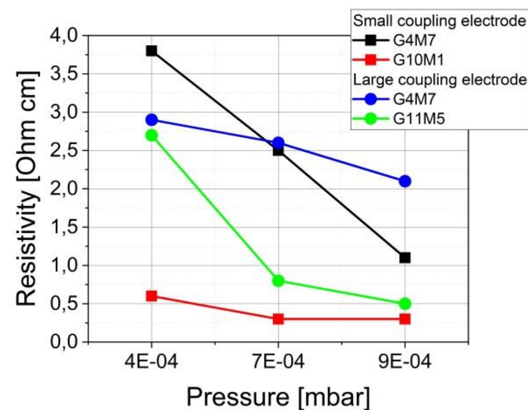

Figure 11: Electrical resistivity of a-C:H:N films deposited on Kapton tape at a substrate temperature of ~ 270°C as a function of pressure for the small and large coupling electrode for magnetic coil settings with a high deposition rate (G10M1 and G11M5) and for a low deposition rate (G4M7). (Distance substrate-extraction grid: 8 cm).

According to Fig. 11, the lowest electrical resistivity value which could be achieved for a-C:H:N films was 0.3 Ohm cm. In our own paper from 2019 [5] we published 1 Ohm cm for a-C:H:N films, which was already a factor of 1000 smaller compared to values from other literature sources for a-C:H:N films [18]. As a reference, pure graphite shows an electrical resistivity of 6.5×10^{-5} Ohm cm (1.5×10^{6} S/m) [19].

IV. Conclusion

Electrically conductive carbon films, a-C:H:N films, were prepared using a plasma beam source. In order to optimize the PACVD deposition process and obtain highly conductive films at high deposition rates, the confining magnetic field was varied. In addition, the influence of substrate temperature, total pressure and RF power on the deposition process was investigated. The following conclusions can be drawn from these studies:

- The deposition rate can be doubled by optimizing the plasma confining magnetic field, and it is further doubled by using a small coupling electrode, i.e. a smaller A_C/A_A ratio. Increasing the RF power does not increase the deposition rate because of increased resputtering by energetic ions and chemical sputtering by ionized nitrogen species. The highest measured deposition rate was 2.4 µm/h (small coupling electrode, $4x10^{-4}$ mbar).
- About twice as much ion energy is generated with the large coupling electrode

as with the small coupling electrode. The variation of the confining magnetic field contributes only about 10% to a change of the ion energy. A change in the total pressure ($4x10^{-4}$ to $9x10^{-4}$ mbar) also affects the ion energy by about 10%. The increase of the RF power leads to a dramatic increase in ion energy. This effect is much stronger with the larger coupling electrode.

- In the pressure range studied ($4x10^{-4}$ to $9x10^{-4}$ mbar) a strong influence of the coupling electrode used (i.e. of the A_C/A_A ratio) and the confining magnetic field on the film hardness was observed. The hardness was in the range of 700-1600 HV. A higher hardness could be achieved by a suitable choice of ion energy and a lower substrate temperature. However, this was not the objective of this work.
- Optimization of the PACVD process parameters, especially variation of the confining magnetic field, led to a reduction of the electrical resistivity of the a-C:H:N films. The lowest value that could be achieved was 0.3 Ohm cm (small coupling electrode, $9x10^{-4}$ mbar).

Compared to the values published in a previous paper by our group [5], both the deposition rate and the electrical resistivity of the a-C:H:N coatings were successfully improved by a factor of 3, respectively.

V. Acknowledgements

The IGF-project 42 EWN of the research association “Research Institute for Precious Metals and Metals Chemistry e.V.” (fem) was funded via the AiF in the frame of the program to promote industrial research and development (IGF) of the Federal Ministry of Economics and Energy based on a decision of the German Parliament. Furthermore, we thank the HS-Group for the loan of the PBS and M. Balzer, P. Neher and L. Schmalz (all fem) for performing and evaluating hardness tests and 4-point-probe measurements.

VI. References

[1] T. Schlößer, "Reversible Brennstoffzelle bricht Wirkungsgrad-Rekord," 18. 12. 2018. [Online]. Available: https://www.fz-juelich.de/de/aktuelles/news/pressemitteilungen/2018/2018-12-18-brennstoffzelle-wirkungsgrad-weltrekord. [Accessed 5. 6. 2023].

[2] L. Fan, Z. Tu and S. Chan, "Recent development of hydrogen and fuel cell technologies: A review," *Energy Rep.,* no. 7, pp. 8421-8446, 2021.

[3] R. Taherian, "A review of composite and metallic bipolar plates in proton exchange," *J. Power Sources,* vol. 265, pp. 370e-390, 2014.

[4] VDI, *VDI-Richtlinien: VDI 2840: Kohlenstoffschichten - Grundlagen, Schichttypen und Eigenschaften,* 2012.

[5] M. Fenker, J. Julin, K. Petrikowski and A. Richter, "Physical and electrical properties of nitrogen-doped hydrogenated amorphous carbon films," *Vacuum 162,* pp. 8-14, 2019.

[6] S. Sattel, M. Weiler, J. Gerber, T. Giessen, H. Roth, et al., "Nucleation during deposition of hydrocarbon ions as a function of substrate temperature," *Diam. Relat. Mater. 4,* pp. 333-336, 1995.

[7] S. Sattel, T. Gießen, H. Roth, M. Scheib, R. Samlenski, R. Brenn, H. Erhardt and J. Robertson, "Temperature dependence of the formation of highly tetrahedral a-C:H," *Diamond Relat. Mater. 5,* pp. 425-428, 1996.

[8] S. Silva, . J. Robertson, G. Amaratunga, B. Rafferty, L. Brown, J. Schwan, et al., "Nitrogen modification of hydrogenated amorphous carbon films," *J. Appl. Phys.,* vol. 81, no. 6, p. 2626–2634, 1997.

[9] *HS-Group GmbH, Manual of Plasma Beam Source PBS 200,* 2009.

[10] H. Oechsner, "Low energy plasma beams for semiconductor technology," *P.F. Williams (ed.) Plasma Processing of Semiconductors, Kluwer Academic Publisher. Netherlands,* 1997.

[11] S. Sattel, *Strukturbildung und Eigenschaften plasmastrahldeponierter Kohlenstoffschichten,* Dissertation, Universität Kaiserslautern, 1996.

[12] J. Vossen, "Glow Discharge Phenomena in Plasma Etching and Plasma Deposition," ***J. Electrochem. Soc.,*** vol. 126, no. 2, p. 319–324, 1979.

[13] G. Sauerbrey, "Verwendung von Schwingquarzen zur Wägung dünner Schichten und zur Mikrowägung," *Z. Phys.,* vol. 155, no. 2, pp. 206-222, 1959.

[14] Y. Yamamura and H. Tawara, "Energy Dependence of Ion Induced Sputtering Yields from Monatomic Solids at normal Incidence," ***At. Data Nucl. Data Tables****62, No. 0005,* pp. 149-253, 1996.

[15] S. E. Rodil, A. Morrison, J. Robertson and I. Milne, "Nitrogen Incorporation into Tetrahedral Hydrogenated Amorphous Carbon," *Phys. Stat. Sol. (a) 174,* pp. 25-37, 1999.

[16] P. Hammer, M. A. Baker, C. Lenardi and W. Gissler, "Ion beam deposited carbon nitride films: characterization and identification of chemical sputtering," *Thin Solid Films 290-291,* pp. 107-111, 1996.

[17] J. Robertson, "Diamond-like amorphous carbon," *Mater. Sci. Eng. R 37,* pp. 129-281, 2002.

[18] J. Schwan, V. Batori, S. Ulrich, H. Ehrhardt and S. Silva, "Nitrogen doping of amorphous carbon thin films," *J. Appl. Phys.,* vol. 84 , no. 4, p. 2071–2081, 1998.

[19] CRC, *Handbook of Physics and Chemistry,* no. 67th, p. 1987, 1986.

Open Access. This article is licensed under a Creative Commons Attribution 4.0 International License, which permits use, sharing, adaptation, distribution and reproduction in any medium or format, as long as you give appropriate credit to the original author(s) and the source, provide a link to the Creative Commons license, and indicate if changes were made. The images or other third party material in this article are included in the article s Creative Commons license, unless indicated otherwise in a credit line to the material. If material is not included in the article's Creative Commons license and your intended use is not permitted by statutory regulation or exceeds the permitted use, you will need to obtain permission directly from the copyright holder. To view a copy of this license, visit: http://creativecommons.org/licenses/by/4.0/.